Supporting Information

HD-ALP Fluorescent Probe: A High-Sensitivity Tool for Alkaline Phosphatase Imaging and Preclinical Diagnosis in Three Ovarian Cancer Models

Yingxian Shi[a,c,1], Ruirui Dong[a,1], Huan Huang[a,c], Gaoying Wang[a], Jianyi Gao[a], Kai Wang[b,*] and Ting Zhang[a,c,*]

[a] Wuxi Maternity and Child Health Care Hospital, Affiliated Women's Hospital of Jiangnan University, Wuxi 214002, China;

[b] Affiliated Children's Hospital of Jiangnan University, Wuxi, 214023, China;

[c] Wuxi School of Medicine, Jiangnan University, Wuxi 214122, China;

[1] These authors contributed equally to this work.

[*]Corresponding author E-mail: 9862022078@jiangnan.edu.cn; hyxj0309@163.com

Experimental protocols

General and measurements

A stock solution (1.0 mM) of **HD-ALP** was prepared in DMSO. Other stock solutions (thiols, anions, cations, and amino acids) were prepared in ultrapure water. Other concentrations were prepared from the dilution. The fluorescence spectral experiments were completed in PBS buffer (10 mM, 1% DMSO, pH 7.4). The excitation wavelength was set as 680 nm. The excitation and emission slit widths were set as 5 nm*5 nm, while the voltage of the photomultiplier was set as 700 V. The error bars displayed the standard deviations from three independent assays.

For cell fluorescence imaging, the IVIS spectral imaging system was used: Imaging parameters: Fluorescence; excitation wavelength of 640 nm and an emission wavelength of 690-770 nm; Field of view: B; Software: Living Image 4.0 software.

Chemical synthesis

2, 3, 3-Trimethyl-3*H*-indolenine (compound **1)** and iodomethane were added to

acetonitrile in a round flask, then the mixture was refluxed for 12 h. Next, the mixture was filtered, and the solid was washed with PE to acquire coarse product compound **3**, which required no further purification for the next step.

A solution of anhydrous DMF and anhydrous DCM was placed in a 150 ml round bottom flask. The solution was cooled and stirred for 20 min, and $POCl_3$ and anhydrous DCM were added dropwise to the above solution by constant pressure drop through a liquid funnel. Cyclohexanone (compound **2**) was added in batches and the solution immediately changed from colorless to yellow. The solution was then slowly heated to 45 °C for a continuous reaction of 3 h. After cooling, the solution was poured into a large amount of ice and left to stand overnight. Yellow compound **4** was obtained.

Compound **3** and compound **4** were dissolved in 100 mL of a mixture of n-butanol and benzene (7:3, v/v) in a 150 mL round flask, refluxed for 3 h, and dried in vacuo to give a green solid. The crude product was purified by silica gel chromatography to give compound **5**.

K_2CO_3 was added in one portion to a round bottom flask containing 3-hydroxyphenol and ACN under a nitrogen atmosphere. The reaction mixture was stirred at room temperature for 10 min and compound **5** was dissolved in ACN and added to the mixed solution. The reaction mixture was heated at 50 °C for 3 h. The solvent was evaporated and the residue was purified by column chromatography to give the desired product **HD**.

A solution of phosphorus oxychloride was gradually added to the solution of **HD** in pyridine and DCM. After stirring at room temperature for 3 h, the mixture was poured into ice water and reacted overnight. Next, the mixture was extracted with DCM and water. Finally, the organic solvent was evaporated, and the residue was purified by silica gel chromatography with CH_2Cl_2/MeOH to obtain **HD-ALP** as a blue solid.

Fluorescence quantum yield

The fluorescence quantum yield Φ was calculated via the relative contrast. According to the standard substance, rhodamine B was prepared in the ethanol

solution. The fluorescence and absorption spectra of rhodamine B and **HD-ALP** were monitored, respectively. Participation ratio assays were conducted using the formula: $\Phi_u = [(A_s F_u n^2)/(A_u F_s n_0^2)] \Phi_s$. The fluorescence quantum yields of **HD-ALP** and rhodamine B were Φ_u and Φ_s. The absorbance values of **HD-ALP** and rhodamine B were A_u and A_s. F_u and F_s referred to their integrated emission band areas. n and n_0 represented the solvent refractive indicators of **HD-ALP** and rhodamine B solutions, respectively.

Control: $\Phi_s = 0.69$, $A_s = 0.016$, $F_s = 179.4$, $n_0 = 1.361$; **HD**: $A_{u1} = 0.022$, $F_{u1} = 199.58$, $n_1 = 1.477$, $\Phi_{u1} = 0.67$; **HD-ALP**: $A_{u2} = 0.019$, $F_{u2} = 13.16$, $n_2 = 1.477$, $\Phi_{u2} = 0.05$.

Limit of detection

The fluorescent emission spectrum of **HD-ALP** in PBS buffer (10 mM, pH = 7.4, 1% DMSO) was recorded 3 times to confirm the background noise σ. The linear regression curve was then fitted according to the data in the range of ALP from 0 U/L to 10000 U/L and obtained the slope of the curve. The detection limit (3σ/slope) was then determined to be 0.238 U/L, which facilitated the quantitative detection of ALP in a complex living body environment.

MTT assays

The cytotoxicity assays were performed on SKOV3 cells and IOSE80 cells. Three replicate wells of the same concentration were used, and each measurement was assayed three times. The cells were grown in a culture medium and treated with various levels of **HD-ALP** for 24 h, 36h and 48h at 37 ℃. Then 10 μL MTT (5 mg/mL) was added to each well and the plate was placed in a 37 ℃ incubator for 4 h. Finally, the cell supernatant was removed and the residue was suspended in 150 μL DMSO. The absorbance was monitored on a Tecan Microplate Reader.

Detection of ALP level of cells

The level of ALP in cell lysates and cell supernatants of SKOV3 and IOSE80 cells was detected by ALP test kit. Three replicate wells of the same concentration were used, and each measurement was assayed three times. The cells were grown in a culture medium for 36h at 37 ℃.

Time-dependent fluorescence imaging in cells

The time-dependent cell imaging was investigated by incubating with **HD-ALP** (20 μM) in cells. The different concentrations of ALP inhibitor Na_3VO_4 were used for treating cells for 30 min. The confocal images of different cells were obtained at different time points by using a laser scanning confocal microscope (set at excitation wavelength 670 nm and collective range from 700-800 nm).

Flow cytometry assays in cells

The flow cytometry(FCM) assays were conducted with **HD-ALP** in living cells. The SKOV3 cells were cultured in 6-well plates at a density of 10^5 cells per well. After the adherence, the subsequent cell treatment methods for each group were similar to those for the fluorescent imaging. After the above steps, the cells were washed three times with PBS, digested with trypsin, and finally suspended with PBS and added to the flow tubes in an ice bath for detection. The results were analyzed with the Flow Jo software.

Imaging in SKOV3-xenograft tumor nude mice models

BALB/C Nude mice (7 weeks old, female) were ordered from Beijing Vital River Laboratory Animal Technology Co., Ltd. (Beijing, China). SKOV3-xenograft tumor mice were established by subcutaneous injection of 10^6 SKOV3 cells into the armpit. All the mice were cared for throughout the experiment. All the animal experimental protocols complied with the requirements of the Ethics Committee of Jiangnan University.

After 15 days, in different groups, the ALP inhibitor Na_3VO_4 was injected intratumorally for 30 min, followed by intratumoral injection of the probe **HD-ALP** (100 μM). These images were captured by the IVIS Lumina XRMS Series III *in vivo* imaging system at different time points of 670 nm excitation and 700 nm to 800 nm emission windows.

Imaging in transgenic primary ovarian mor mice model

C57BL/6J mice (8 weeks old, female) were ordered from Beijing Vital River Laboratory Animal Technology Co., Ltd. (Beijing, China). The model mice were established by injecting inducers Akt/Myc oncogene plasmid combination. All mice

were cared for throughout the experiments. All the animal experimental protocols complied with the requirements of the Ethical Committee of Jiangnan University.

After 20 days, in different groups, the ALP inhibitor Na_3VO_4 was injected intraperitoneally for 30 min, followed by tail vein injection of the **HD-ALP** (100 μM). These images were captured by the IVIS Lumina XRMS Series III *in vivo* imaging system at different time points of 670 nm excitation and 700 nm to 800 nm emission windows.

Imaging in in-situ ovarian tumor mice model

BALB/C Nude mice (7 weeks old, female) were ordered from Beijing Vital River Laboratory Animal Technology Co., Ltd. (Beijing, China). The *in-situ* ovarian tumor model mice were established by *in-situ* inoculation of 10^6 SKOV3 cells into the ovarian area. All the mice were cared for throughout the experiment. All the animal experimental protocols complied with the requirements of the Ethics Committee of Jiangnan University.

After 21 days, in different groups, the ALP inhibitor Na_3VO_4 was injected intraperitoneally for 30 min, followed by tail vein injection of the **HD-ALP** (100 μM). These images were captured by the IVIS Lumina XRMS Series III *in vivo* imaging system at different time points of 670 nm excitation and 700 nm to 800 nm emission windows.

Detection of serum indexes

The normal and model mice were involved. The blood was collected from the orbit and placed in the centrifuge tube at 4 ℃ for 2 h. The supernatant was obtained by centrifugation for 15 min at 4 ℃, 3500 rpm. Then the supernatant was centrifuged for 10 min under the condition of 4 ℃, 3500 rpm. The levels of CA125 and HE4 in the serum of mice in each group were detected by ELISA test kit. Finally, the serum from the same group of three model mice were mixed, then,the levels of ALP in the serum was detected by an automatic biochemical analyzer.

Histopathological examination

Staining of the tissue section: Different tissues were fixed in 10% formalin

solution for 24 h, dehydrated and cleated, then waxed, embedded, and cut into 5 μm paraffin sections. The paraffin sections were dewaxed and rehydrated, stained with HE, and pathologically analyzed under a microscope. Immunohistochemical labeling corresponds to positive staining of antibodies under a microscope.

Supplementary figures

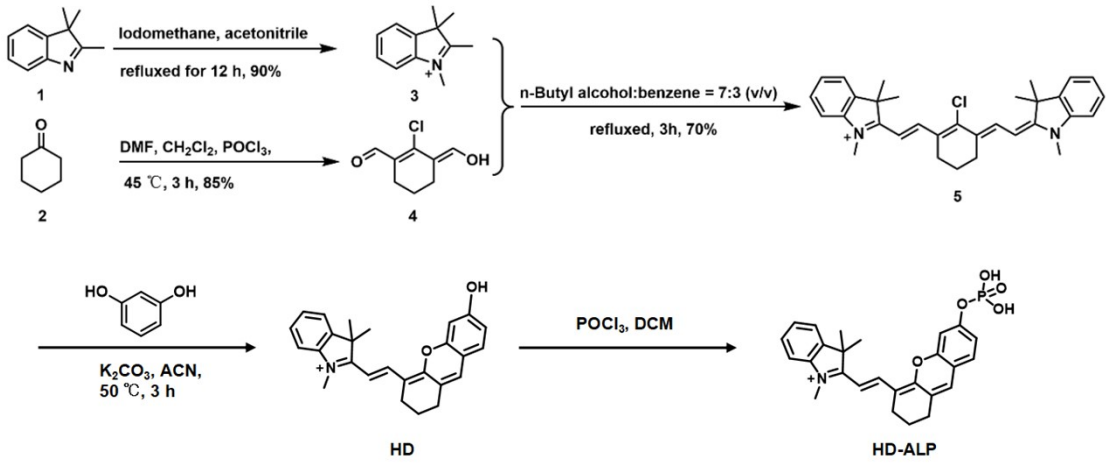

Figure S1. The synthetic route of **HD-ALP**.

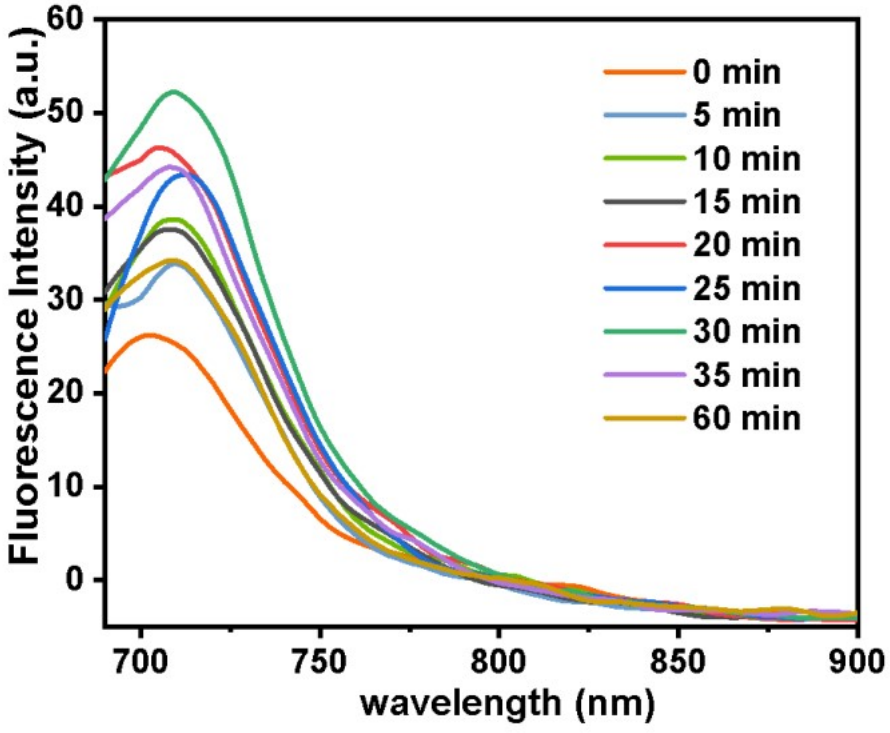

Figure S2. The fluorescence intensity of different time points with **HD-ALP** in

presence of ALP.

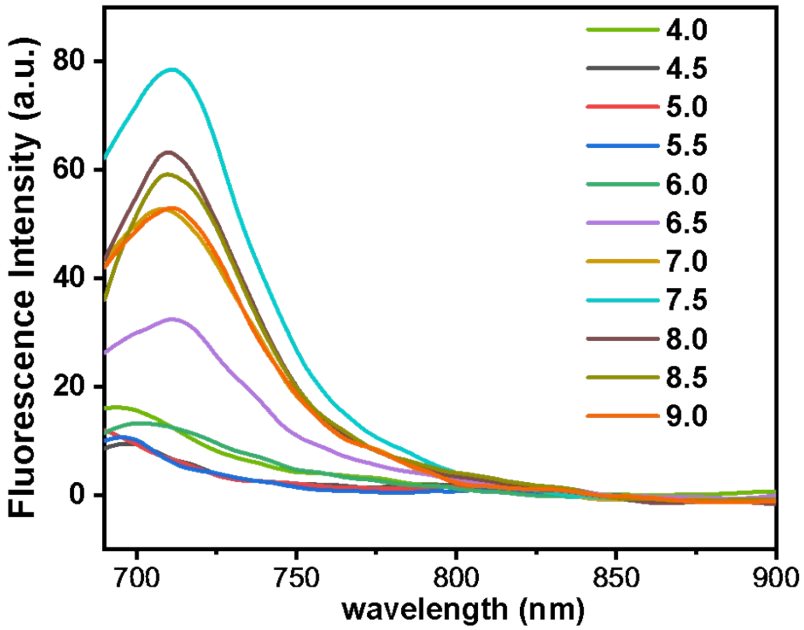

Figure S3. The fluorescence intensity of different pH with **HD-ALP** in presence of ALP.

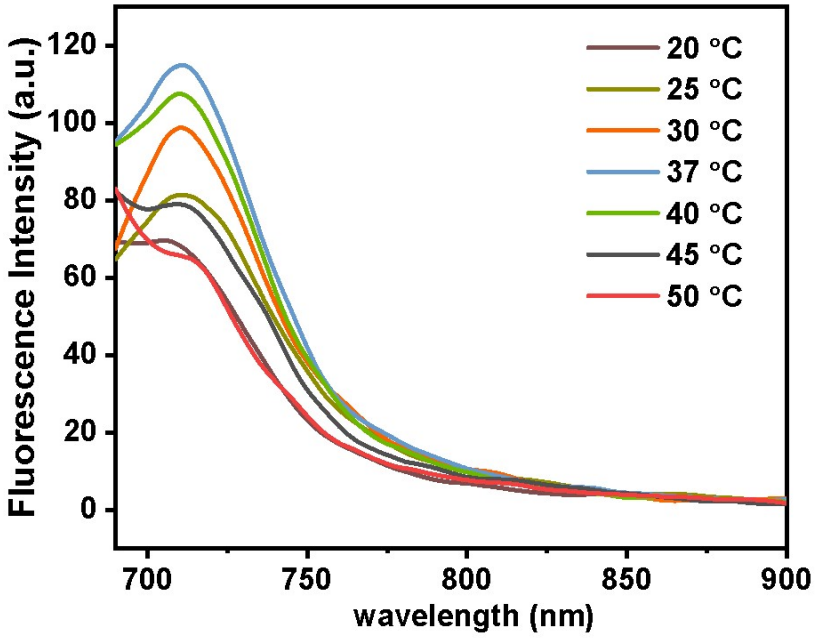

Figure S4. The fluorescence intensity of different temperatures with **HD-ALP** in presence of ALP.

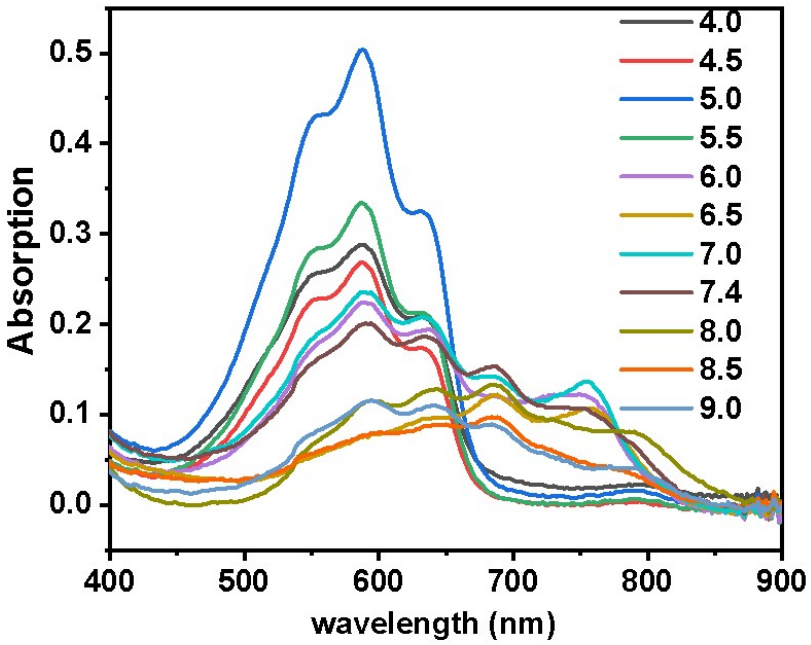

171

172 **Figure S5.** The absorption of different pH with **HD-ALP** in presence of ALP.

173

174

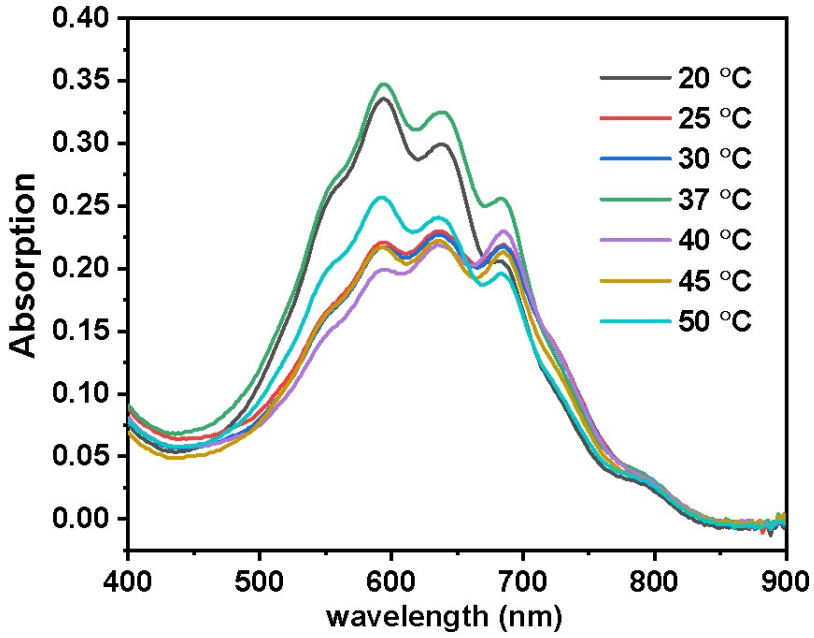

175

176 **Figure S6.** The absorption of different temperatures with **HD-ALP** in presence of

177 ALP.

178

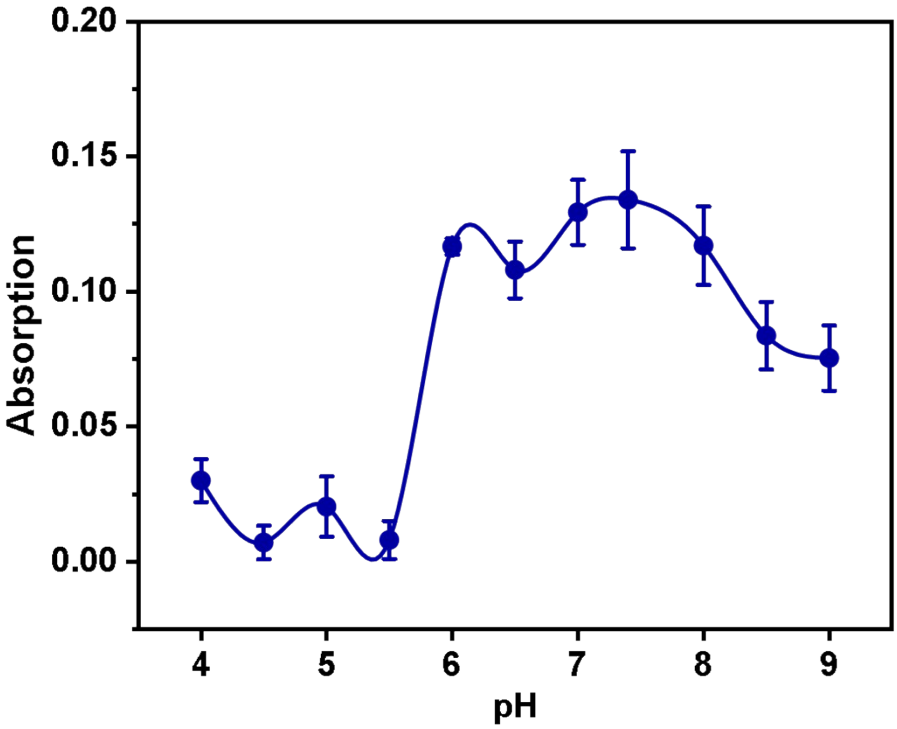

Figure S7. Changes in the absorption of **HD-ALP** at different pH conditions after reacting with ALP.

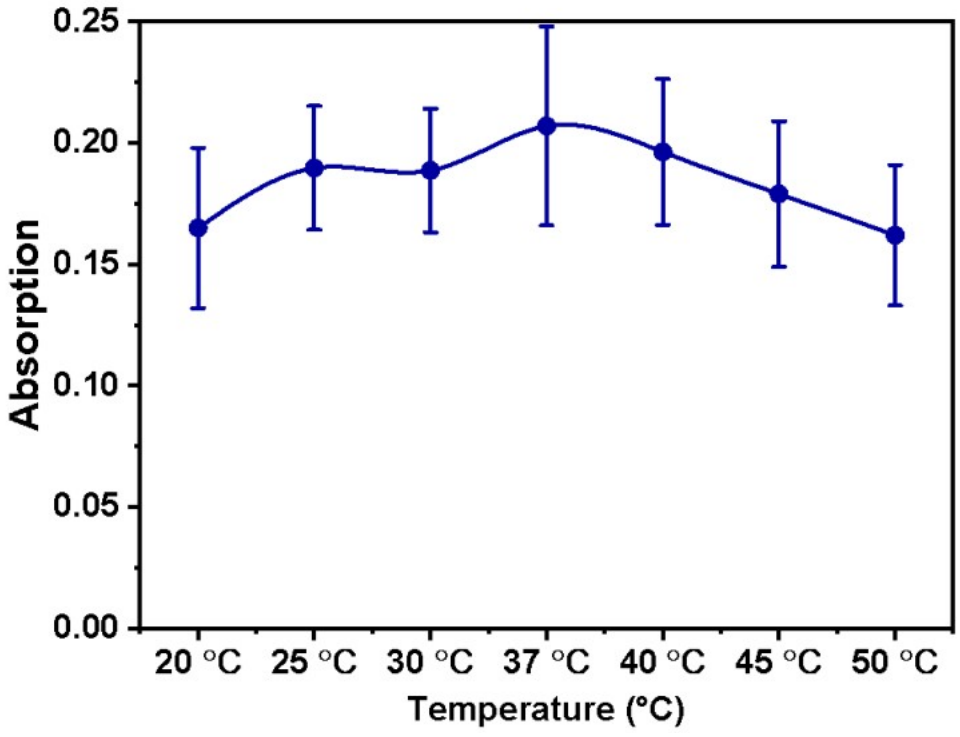

Figure S8. Changes in the absorption of **HD-ALP** at different temperature conditions

after reacting with ALP.

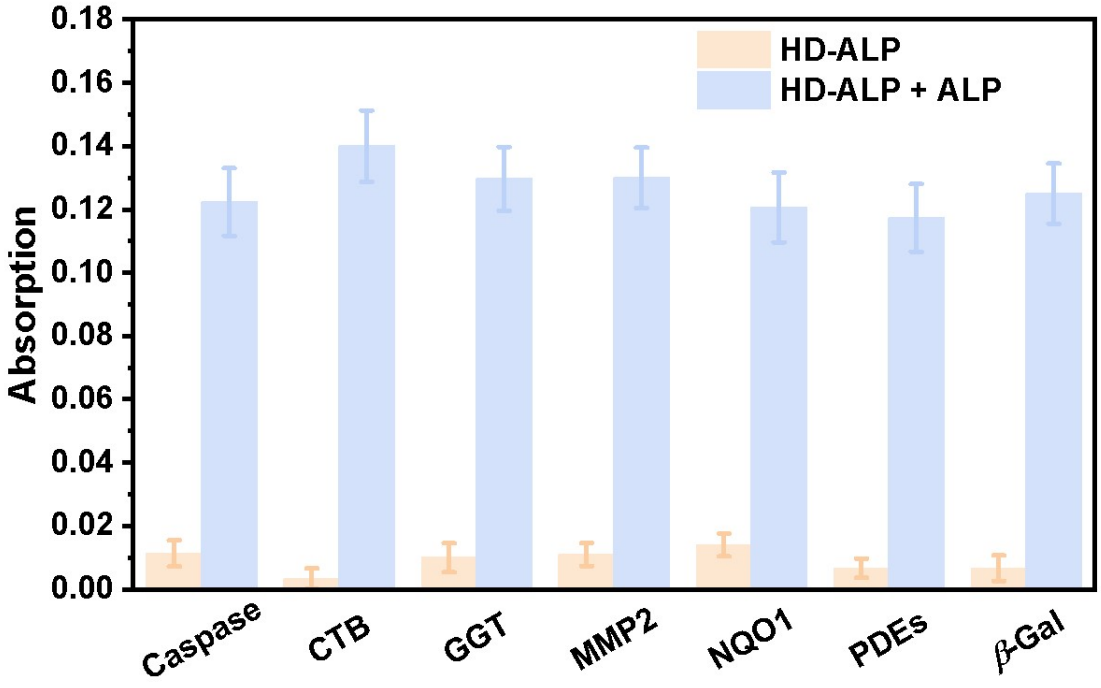

Figure S9. Absorption of **HD-ALP** changes by adding competitive substances (enzymes) and ALP.

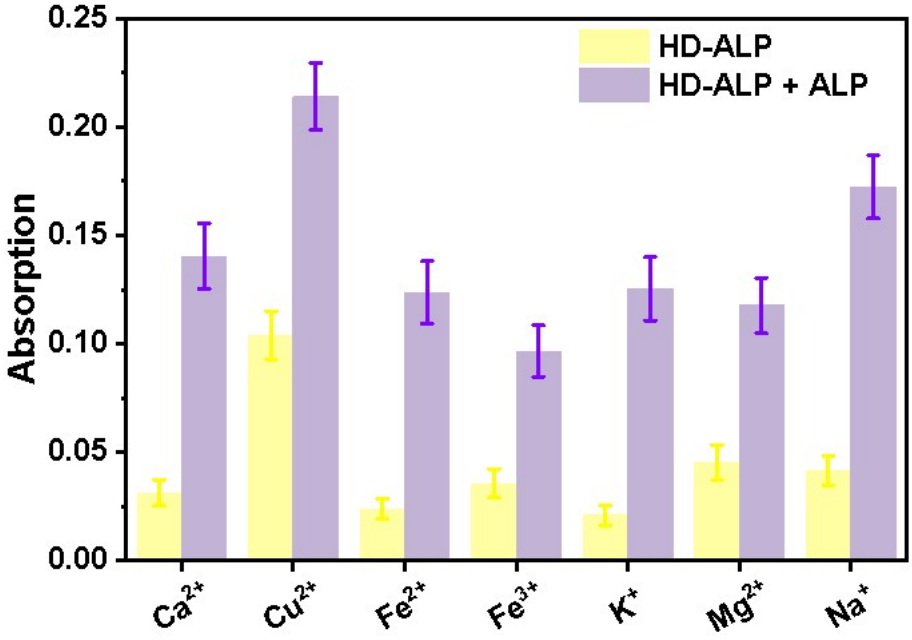

Figure S10. Absorption of **HD-ALP** changes by adding competitive substances (cations) and ALP.

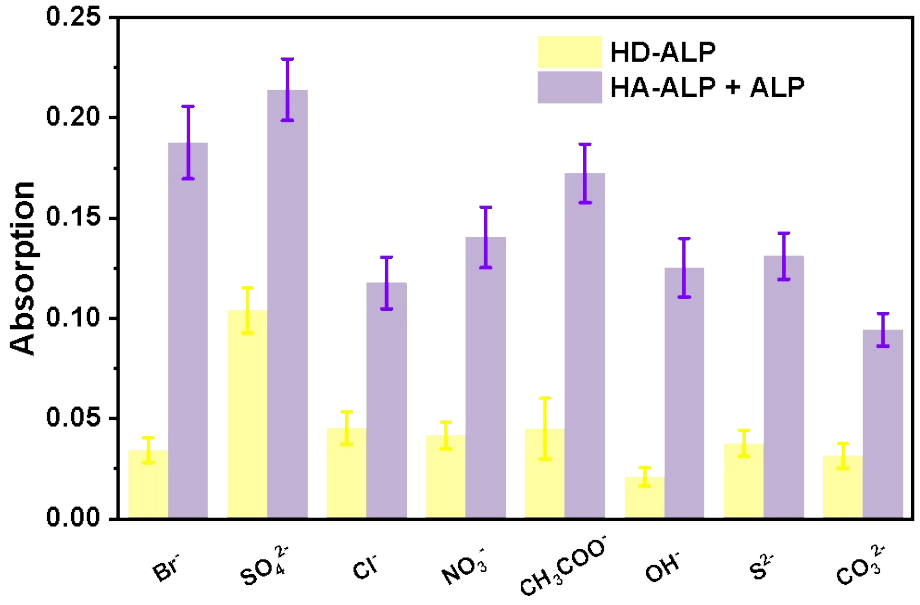

195

196 **Figure S11.** Absorption of **HD-ALP** changes by adding competitive substances

197 (anions) and ALP.

198

199

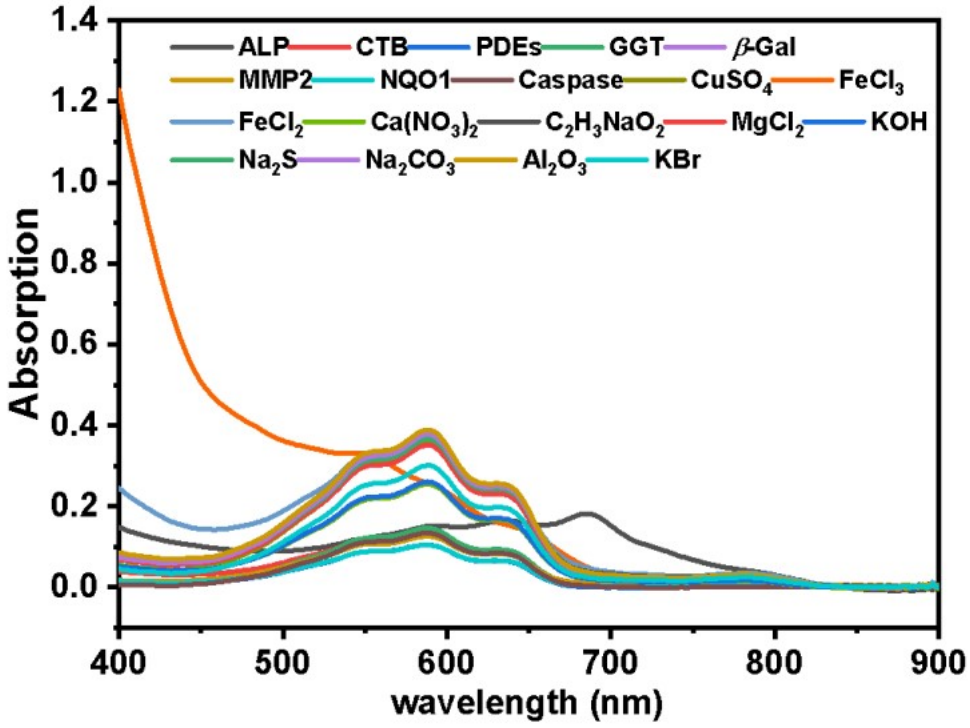

200

201 **Figure S12.** Absorption of **HD-ALP** after the addition of species.

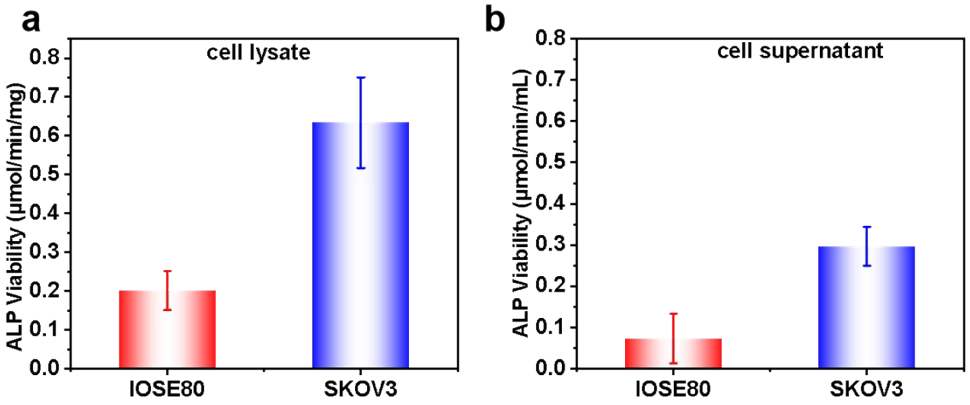

Figure S13. The levels of ALP in cell lysates and cell supernatants

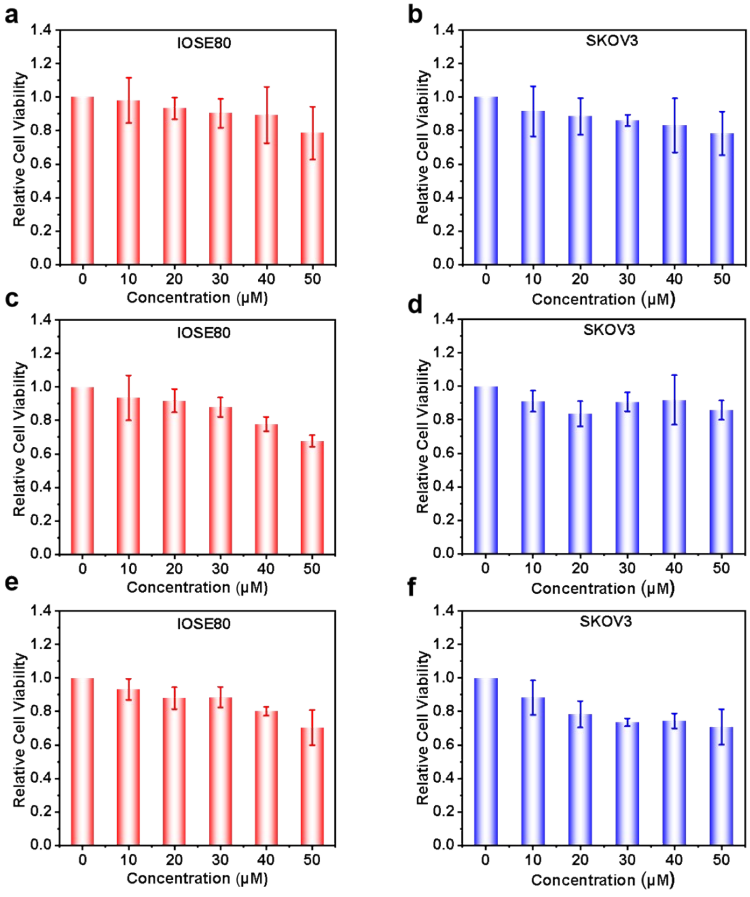

Figure S14. (**a** and **b**) The cell variation of IOSE80 and SKOV3 cells was treated with different concentrations of **HD-ALP** for 24 h. (**c** and **d**) The cell variation of IOSE80 and SKOV3 cells was treated with different concentrations of **HD-ALP** for 36 h. (**e** and **f**) The cell variation of IOSE80 and SKOV3 cells was treated with different concentrations of **HD-ALP** for 48 h.

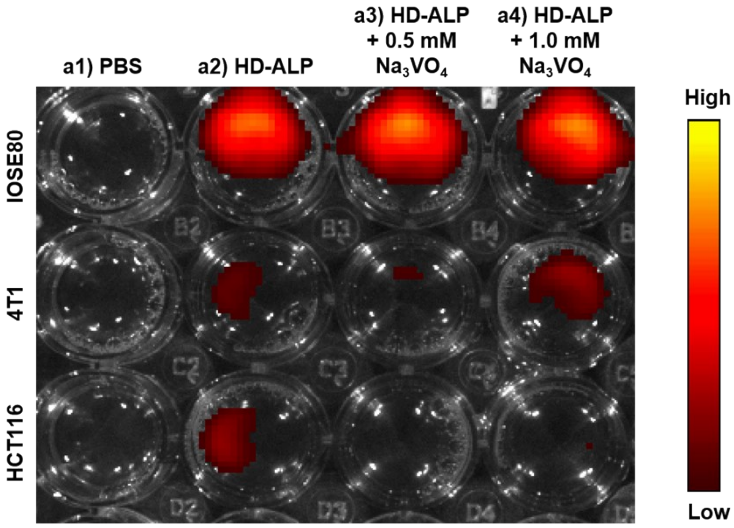

Figure S15. FL images of ALP in IOSE80, 4T1 and HCT116 cells with different concentrations of inhibitor by IVIS images.

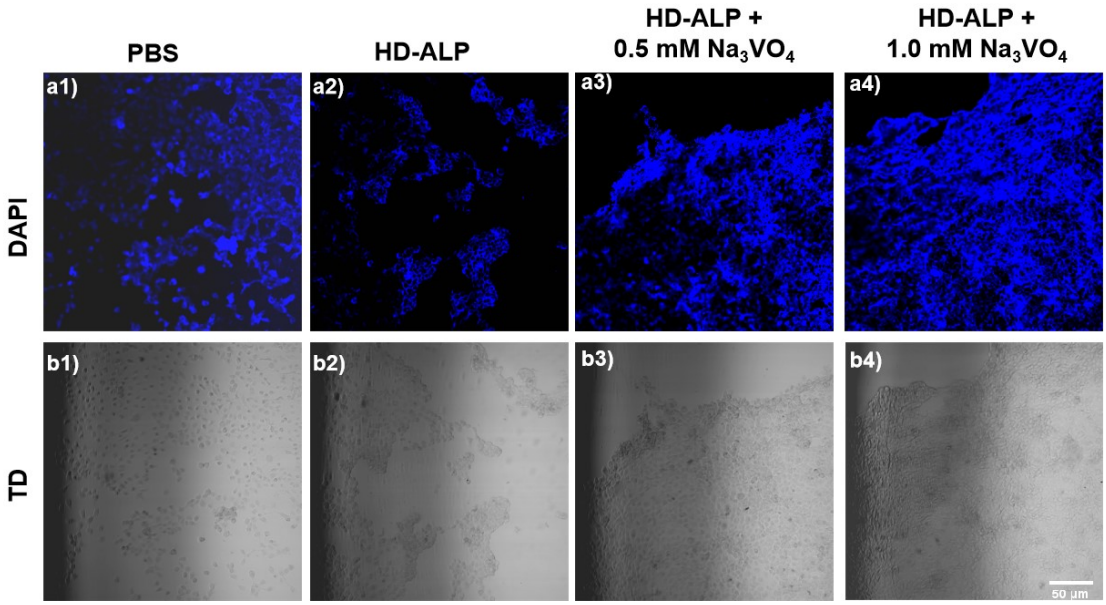

Figure S16. FL Images of ALP in SKOV3 cells by confocal FL images (incubated DAPI and TD), 100×. Scale: 50 μm.

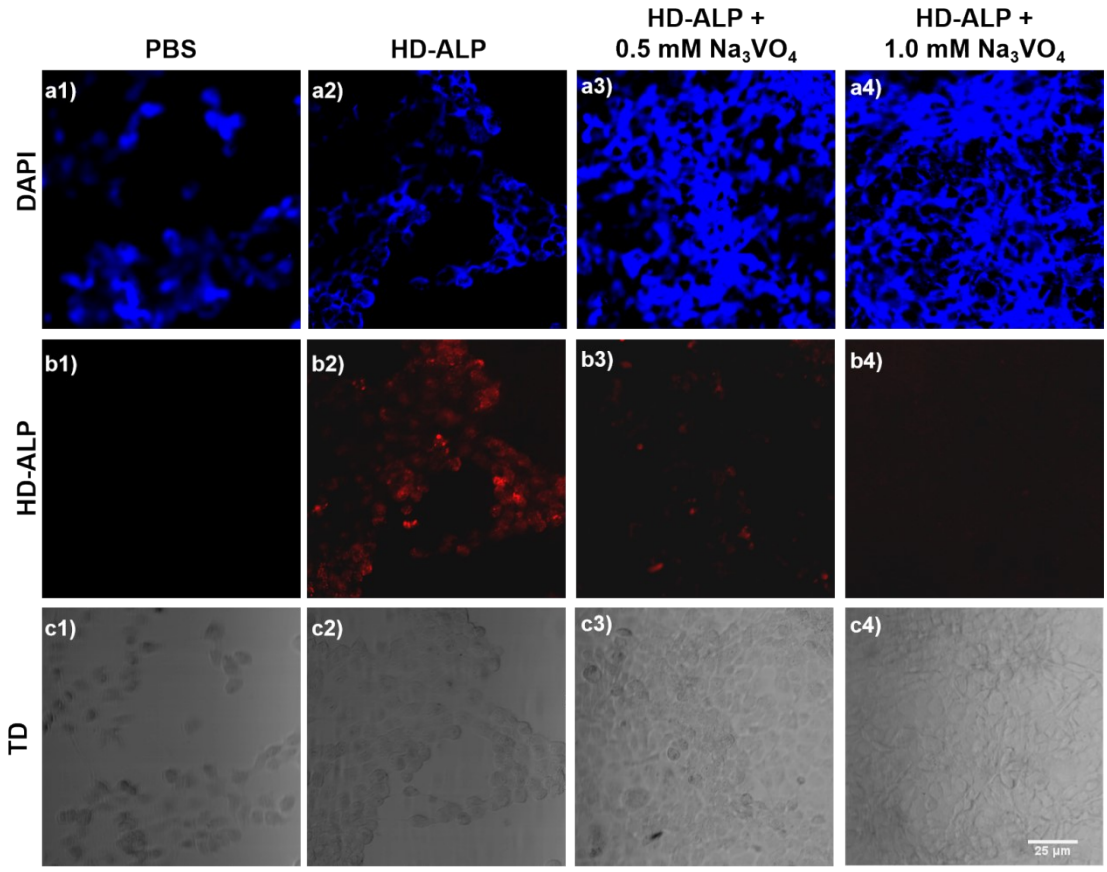

Figure S17. FL Images of ALP in SKOV3 cells by confocal FL images (incubated DAPI, **HD-ALP** and TD), 100×. Scale: 25 μm.

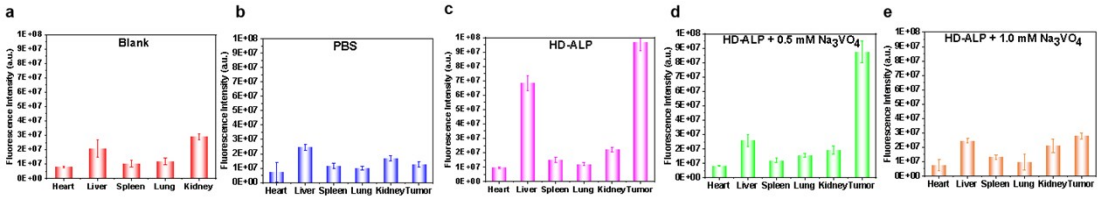

Figure S18. The fluorescence intensity corresponds to each organ's FL imaging of SKOV3-xenograft tumor nude mice models.

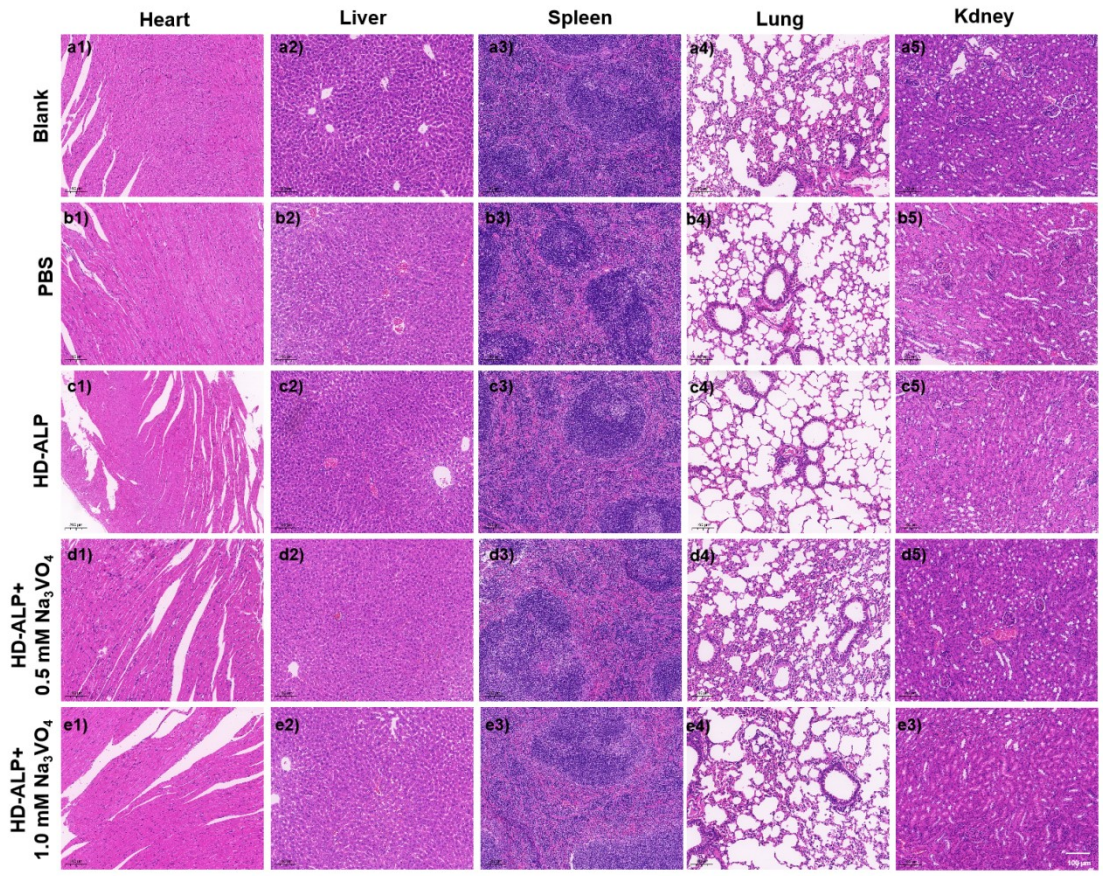

225

226 **Figure S19.** HE staining in major organs of SKOV3-xenograft tumor nude mice

227 models, 200×. Scale: 100 μm.

228

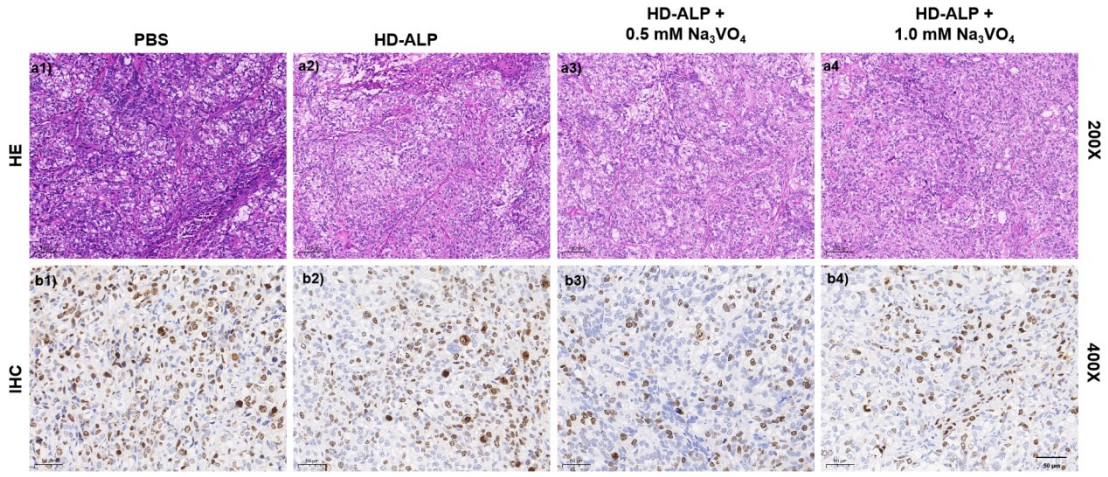

229

230 **Figure S20.** HE and Ki67 immunohistochemical staining of SKOV3-xenograft tumor

231 nude mice models. HE scale: 100 μm, IHC scale: 50 μm.

232

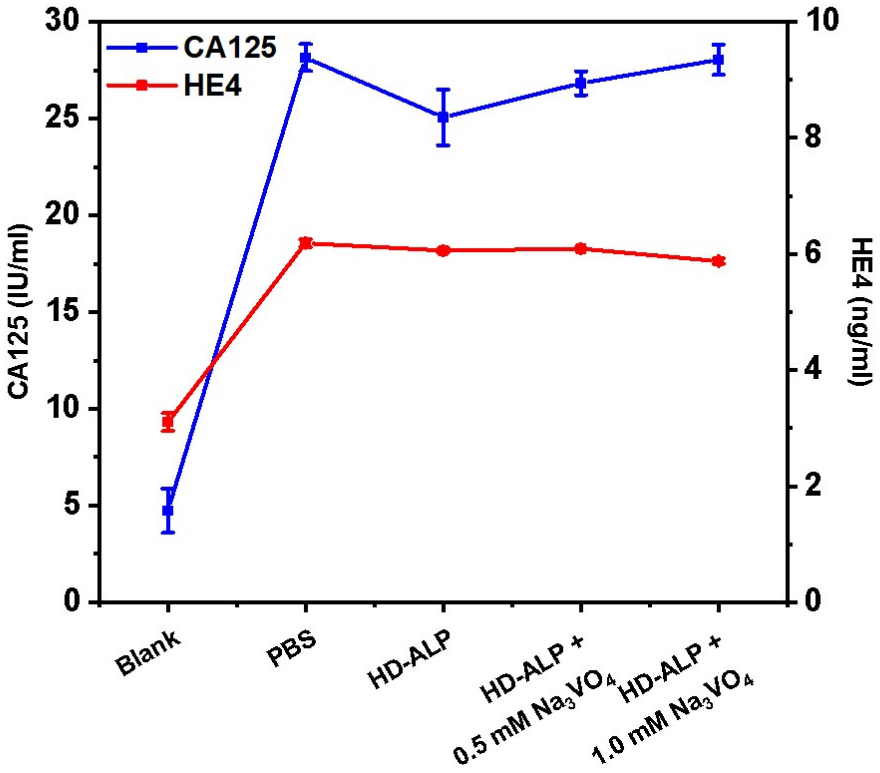

Figure S21. The serum marker test results of CA125 and HE4 of SKOV3-xenograft tumor nude mice models.

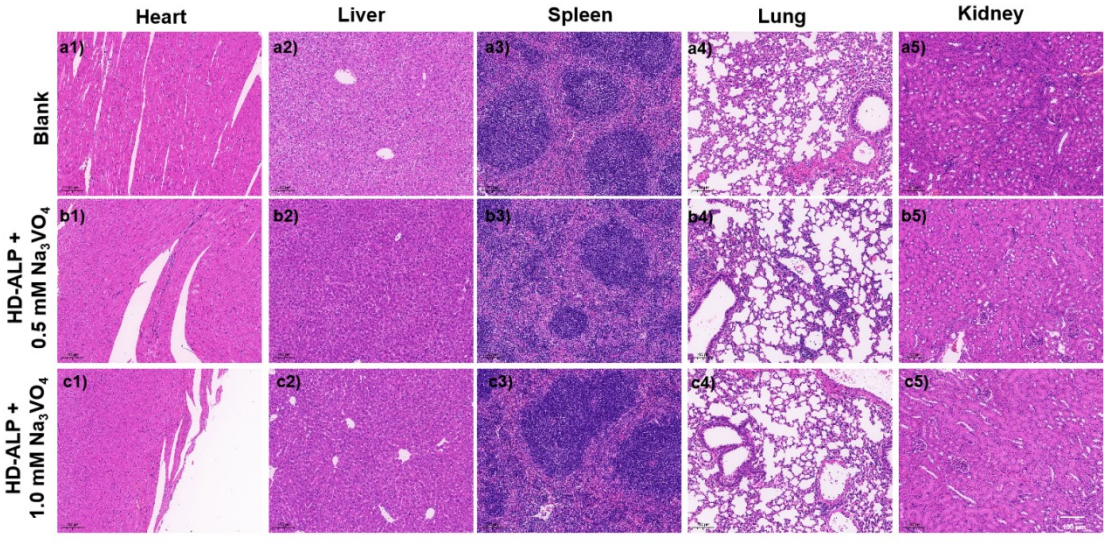

Figure S22. HE staining in major organs of transgenic primary ovarian mor mice models, 200×. Scale: 100 μm.

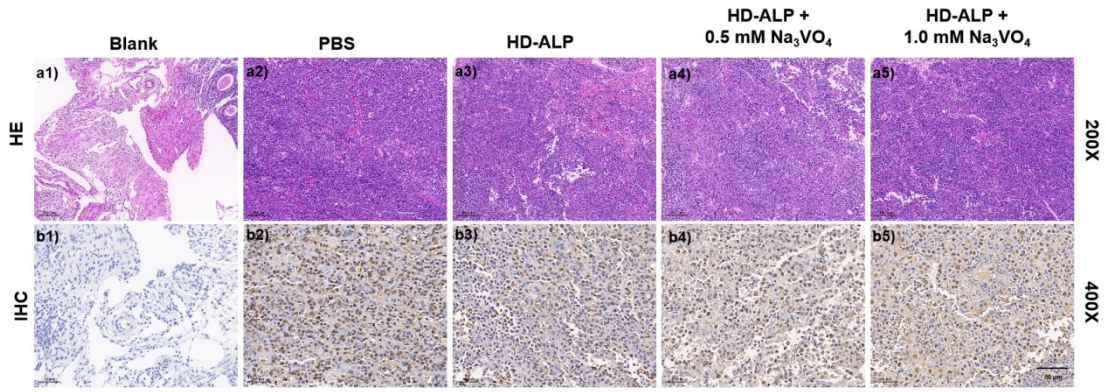

241

242 **Figure S23.** HE and Ki67 immunohistochemical staining of transgenic primary

243 ovarian mor mice models. HE scale: 100 μm, IHC scale: 50 μm.

244

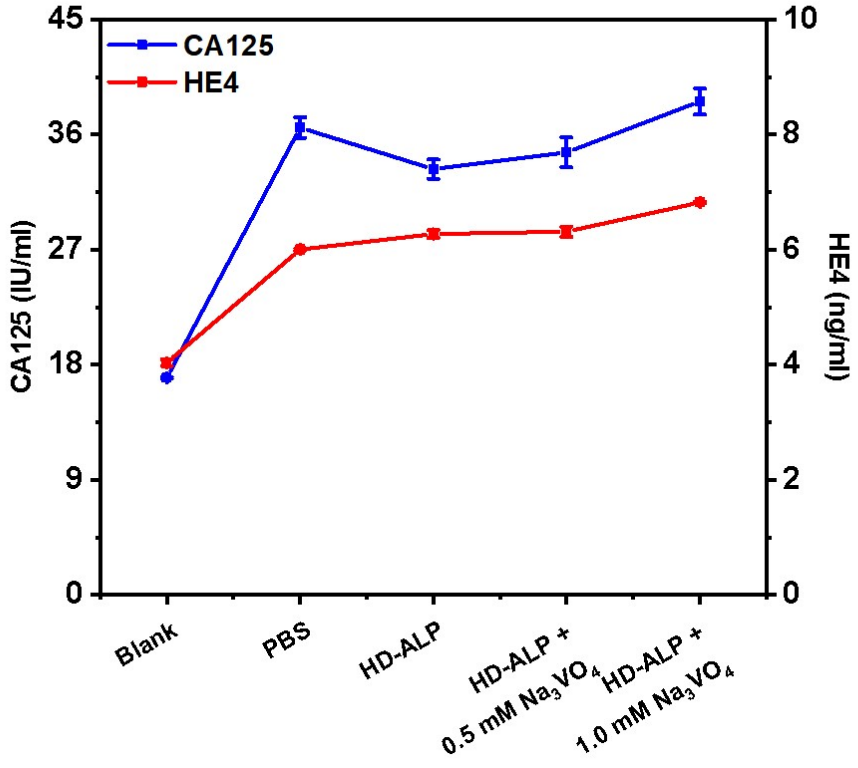

245

246 **Figure S24.** The serum marker test results of CA125 and HE4 of transgenic primary

247 ovarian mor mice models.

248

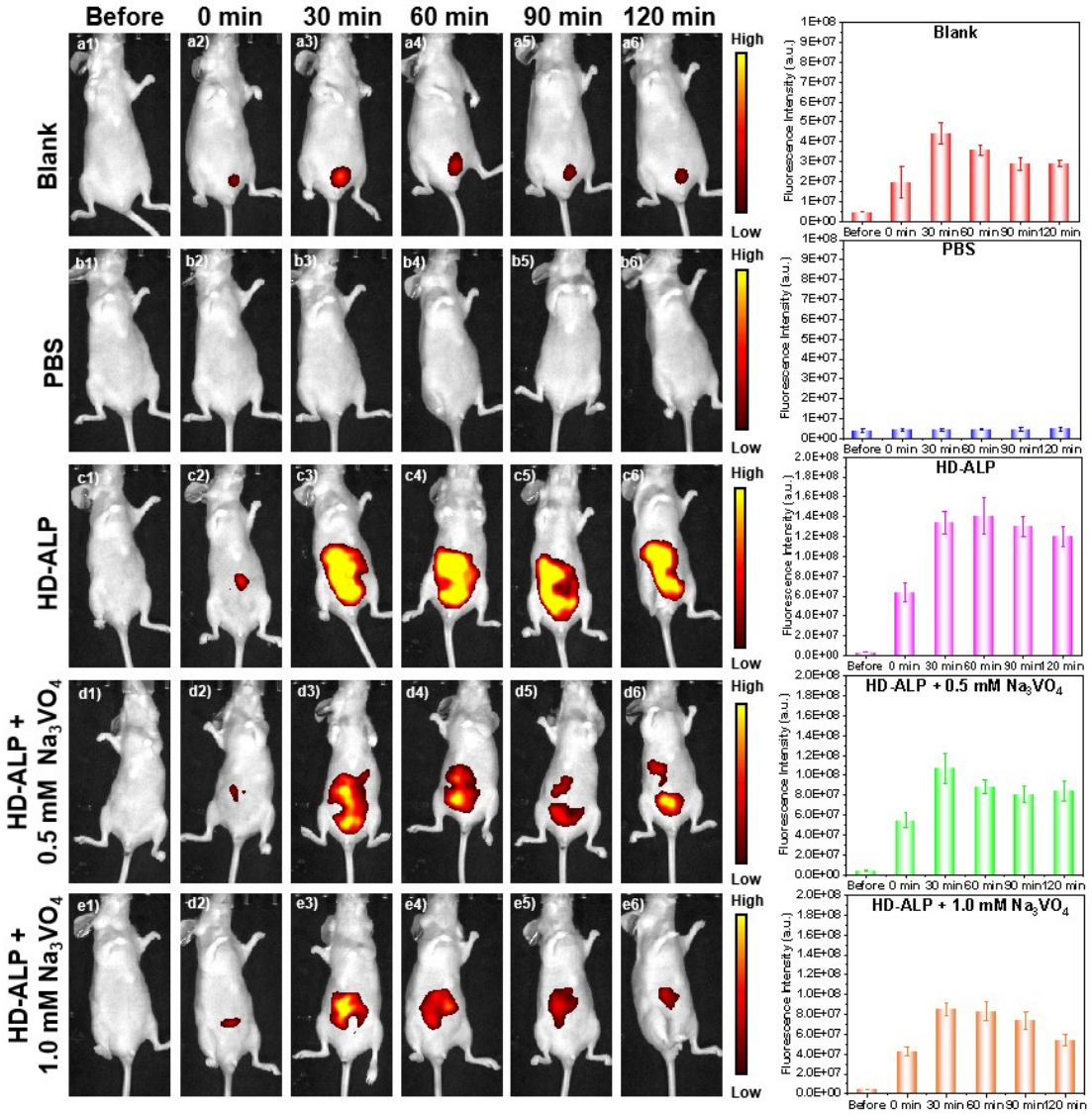

Figure S25. *In vivo* FL imaging at different time points of *in-situ* ovarian tumor mice models and FL imaging of major organs in mice for each group and the fluorescence intensity corresponding to each group's FL imaging.

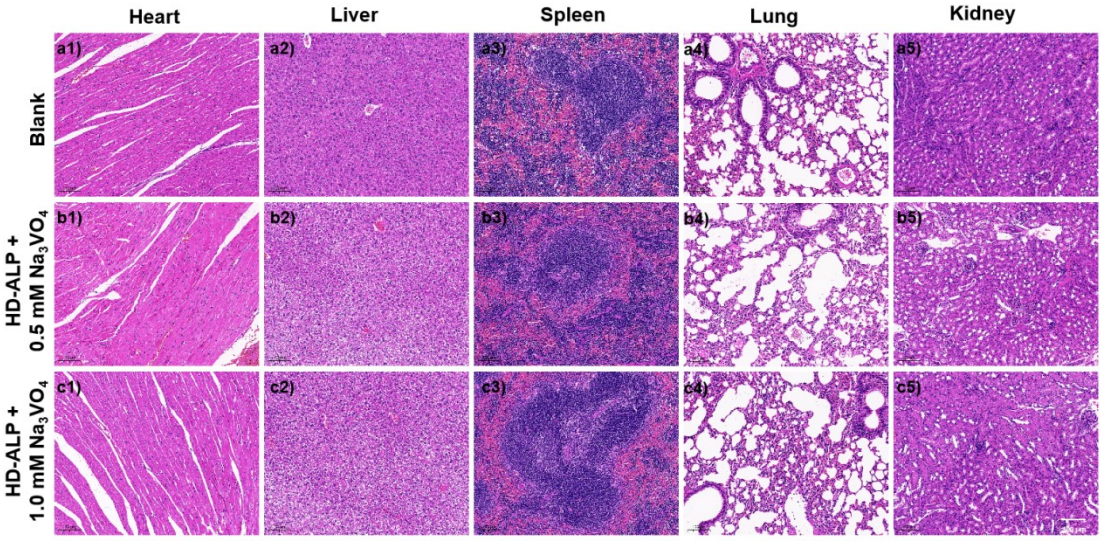

Figure S26. HE staining in major organs of *in-situ* ovarian tumor mice models, 200×. Scale: 100 μm.

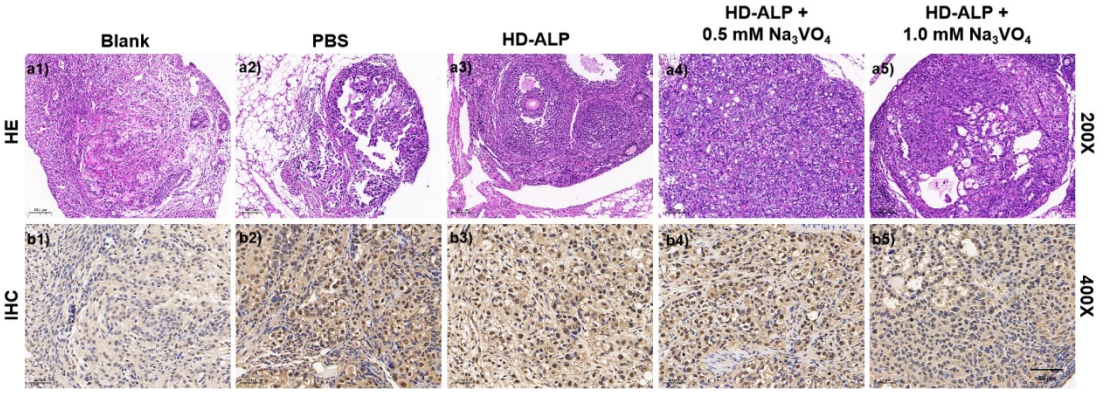

Figure S27. HE and Ki67 immunohistochemical staining of *in-situ* ovarian tumor mice models. HE scale: 100 μm, IHC scale: 50 μm.

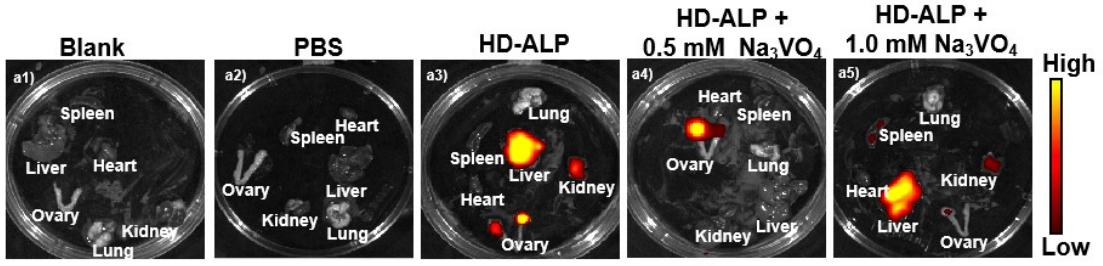

Figure S28. FL imaging of major organs in mice for each group of *in-situ* ovarian tumor mice models.

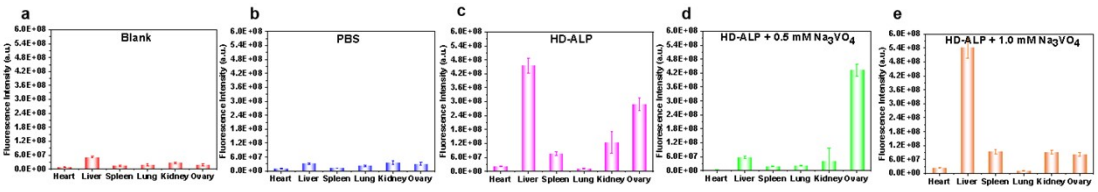

Figure S29. The fluorescence intensity corresponds to each organ's FL imaging of *in-situ* ovarian tumor mice models.

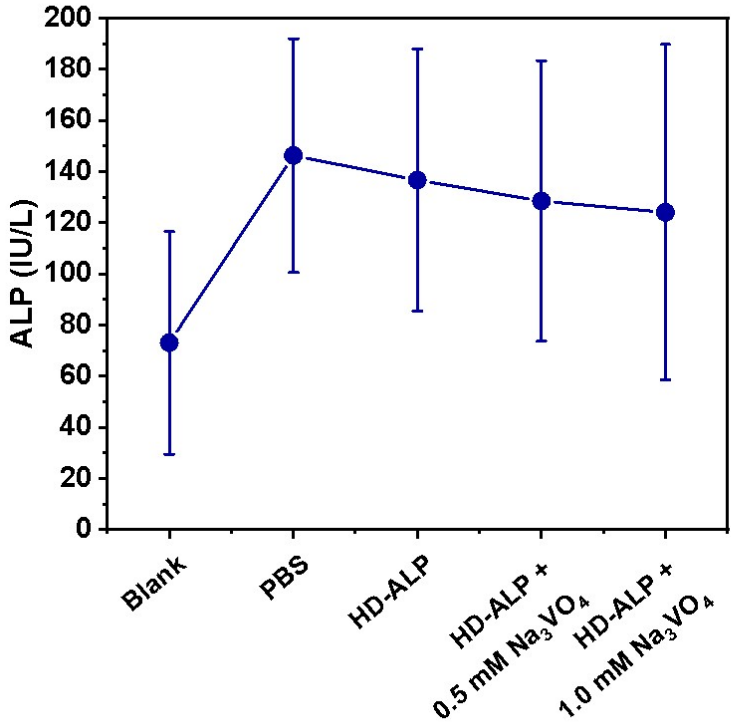

Figure S30. The test results of ALP of the three mice models.

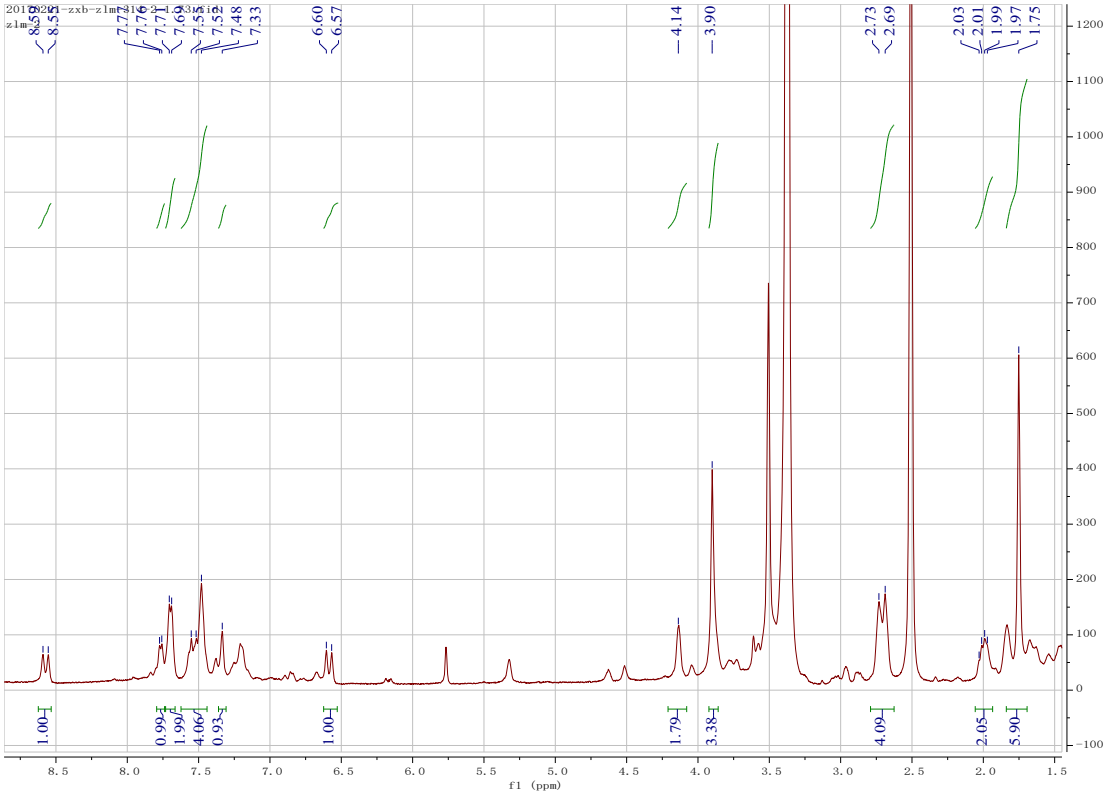

Figure S27. ^{1}H NMR spectrum of **HD-ALP**.

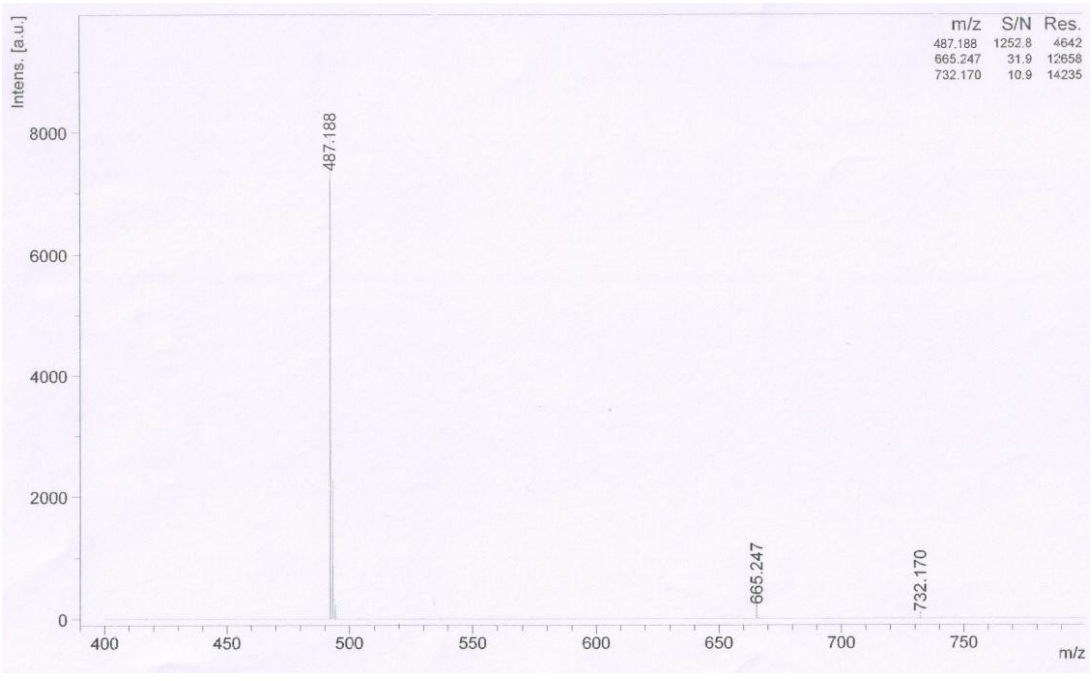

Figure S28. MS mass spectrum of **HD-ALP**.

Table S1. The comparison between **HD-ALP** and previously reported probes.

Probe	$\lambda_{ex}/\lambda_{em}$	Respon	Time	LOD	applicati	Refe

	(nm)	se fold	(min)	(U/L)	on	renc e
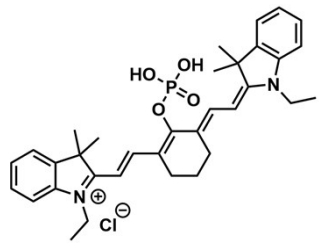	516/616, 736/766	-	30	0.16	Cell	1
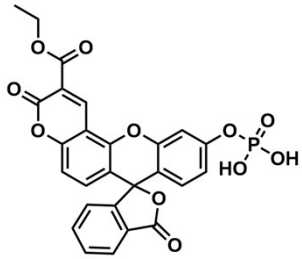	405/465, 530	-	14	0.006	Cell Serum	2
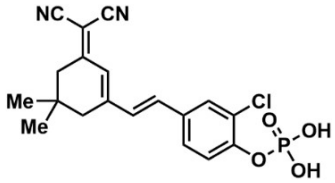	405/670	-	30	0.87	Cell	3
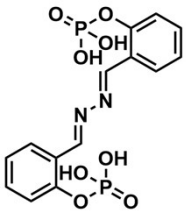	356/536	240	10	0.012	Cell	4
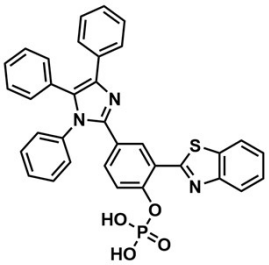	365/550	20	30	1.212 28	Cell	5
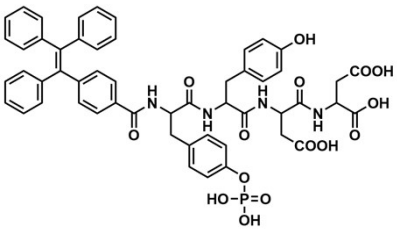	375/480	59	-	0.001 2	Cell	6

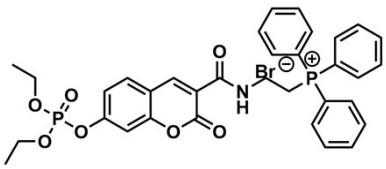	410/450	15	30	2.921	Cell	7
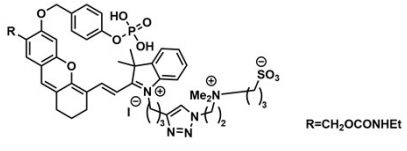	685/720	30	10	-	Cell Mice	8
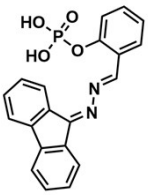	380/585	5	50	0.6	Cell	9
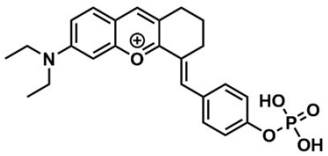	585/655	9	144	-	Cell Tissue	10
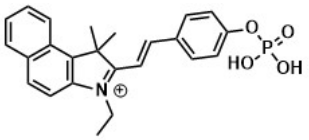	530/575	-	30	0.73	Chlorella E. coli	11
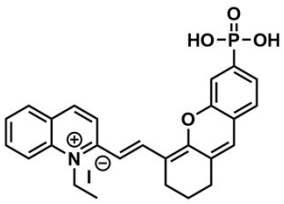	720/770	7	10	0.017	Cell Mice	12
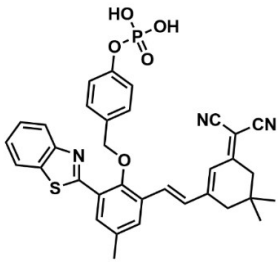	423/689	-	8.5	3.98	Cell Zebrafish	13
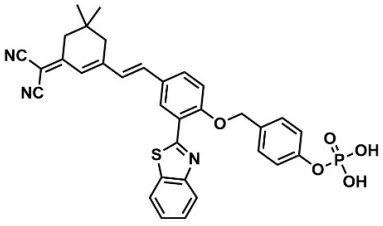	410/550, 670	-	5	2.36	Cell Zebrafish	14

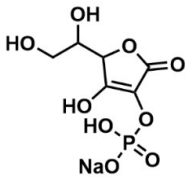	370/389, 536	20	80	0.08	Cell	15
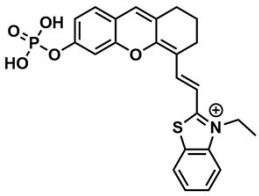	680/723	56	15	0.042	Cell	16
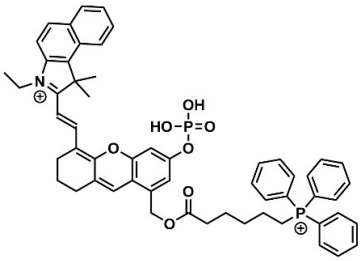	710/735	13.2	20	-	Cell Mice	17
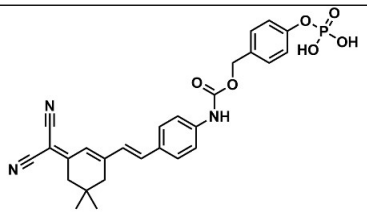	410/580, 650	14	10	0.89	Cell Serum	18
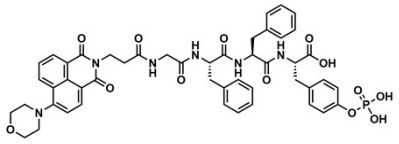	405/	13	180	-	Cell	19
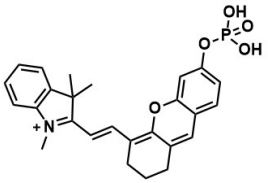	**680/715**	**-**	**30**	**0.238**	**Cell Mice**	**This work**

Reference

[1] Zhang Q, Li S, Fu C, Xiao Y, Zhang P, D. C., Near-infrared mito-specific fluorescent probe for ratiometric detection and imaging of alkaline phosphatase activity with high sensitivity, Journal of Materials Chemistry B 7(3) (2019) 443-450.

[2] J. Cao, Q. Wu, X. Chang, H. Chu, H. Zhang, X. Fang, F. Chen, Ratiometric detection and imaging of endogenous alkaline phosphatase activity by fluorescein-coumarin-based fluorescence probe, Spectrochimica Acta Part A: Molecular and Biomolecular Spectroscopy 281 (2022) 121615.

[3] Y.-A. Feng, H. Xu, Y. Zhou, B.-J. Wang, J. Xiao, Y.-W. Wang, Y. Peng, Ratiometric detection and bioimaging of endogenous alkaline phosphatase by a NIR fluorescence probe, Sensors and Actuators B: Chemical 358 (2022) 131505.

[4] Y. He, J. Yu, X. Hu, S. Huang, L. Cai, L. Yang, H. Zhang, Y. Jiang, Y. Jia, H. Sun, An activity-based fluorescent probe and its application for differentiating alkaline phosphatase activity in different

cell lines, Chemical Communications 56 (2020) 13323-13326.
[5] L. Huang, X. Cao, T. Gao, B. Feng, W. Zeng, A novel aggregation-induced dual emission probe for in situ light-up detection of endogenous alkaline phosphatase, Talanta 225 (2021) 121950.
[6] Q. Jiao, Y. Zheng, S. Pei, X. Luo, X. Wu, K. Xu, W. Zhong, Cascade-Activated AIEgen-Peptide Probe for Noninvasively Monitoring Chymotrypsin-like Activity of Proteasomes in Cancer Cells, Analytical Chemistry 95(23) (2023) 9097-9106.
[7] S. Khatun, S. Biswas, A.K. Mahanta, M.M. Joseph, M.S. Vidyalekshmi, A. Podder, P. Maiti, K.K. Maiti, S. Bhuniya, Biocompatible fluorescent probe for detecting mitochondrial alkaline phosphatase activity in live cells, Journal of Photochemistry and Photobiology B: Biology 212 (2020) 112043.
[8] Y. Li, H. Song, C. Xue, Z. Fang, L. Xiong, H. Xie, A self-immobilizing near-infrared fluorogenic probe for sensitive imaging of extracellular enzyme activity in vivo, Chemical Science 11(23) (2020) 5889-5894.
[9] Y. Li, R. Xie, X. Pang, Z. Zhou, H. Xu, B. Gu, C. Wu, H. Li, Y. Zhang, Aggregation-induced emission fluorescent probe for monitoring endogenous alkaline phosphatase in living cells, Talanta 205 (2019) 120143.
[10] C. Liu, Y. Zhou, Y. Zhao, M. Jia, W. Wang, Y. He, S. Yang, Y. Qiao, L. Duan, Effects of the molluscicide candidate PPU06 on alkaline phosphatase in the golden apple snails determined using a near-infrared fluorescent probe, CHINESE CHEMICAL LETTERS 32(05) (2021) 1809-1813.
[11] J. Sun, MeiWang, PengGao, ZhiweiMu, JunChen, Qingguo, Novel High-Selectivity Fluorescent Probe for Detecting Alkaline Phosphatase Activity in Marine Environment, Journal of nanoscience and nanotechnology 20(6) (2020) 3348-3355.
[12] Wang, Wen-Xin, Jiang, Wen-Li, Hong, Yongfei, Chun-Yan, Real-time imaging of alkaline phosphatase activity of diabetes in mice via a near-infrared fluorescent probe, Chemical Communications 57(04) (2021) 480-483.
[13] L. Wang, S. Chen, X. Ma, Y. Wu, Y. Tang, S. Hou, Fast and sensitive near-infrared ratiometric fluorescent probe with a self-immolative spacer for imaging of endogenous alkaline phosphatase activity in cells and in vivo, Talanta 249 (2022) 123658.
[14] L. Wang, K. Niu, S. Chen, Near-infrared fluorescent probe with a self-immolative spacer for ratiometric imaging alkaline phosphatase in cell and zebrafish, Dyes and Pigments 209 (2023) 110910.
[15] J. Wen, Y. Hu, N. Li, D. Li, G. Zheng, Y. Zou, M. Zhang, L. Shui, In situ fluorogenic reaction for ratiometric fluorescent detection of alkaline phosphatase activity, Analytica Chimica Acta 1230 (2022) 340414.
[16] L. Xu, X. He, Y. Huang, P. Ma, Y. Jiang, X. Liu, S. Tao, Y. Sun, D. Song, X. Wang, A novel near-infrared fluorescent probe for detecting intracellular alkaline phosphatase and imaging of living cells, Journal of Materials Chemistry B 7 (2019) 1284-1291.
[17] D. Yao, S. Yang, Y. Wang, K. Bian, W. Yang, D. Wang, B. Zhang, An ALP-activatable and mitochondria-targeted probe for prostate cancer-specific bimodal imaging and aggregation-enhanced photothermal therapy, Nanoscale 11(13) (2019) 6307-6314.
[18] X. Zhang, X. Chen, K. Liu, Y. Zhang, G. Gao, X. Huang, S. Hou, Near-infrared ratiometric probe with a self-immolative spacer for rapid and sensitive detection of alkaline phosphatase activity and imaging in vivo, Analytica Chimica Acta 1094 (2020) 113-121.
[19] Y. Zhang, Y. Ding, X. Li, Z. Zhang, X. Zhang, Y. Chen, Z. Yang, Y. Shi, Z.W. Hu, Enzyme-

336 instructed self-assembly enabled fluorescence light-up for alkaline phosphatase detection,
337 Talanta 239 (2022) 123078.